

Chapter 2

Theory on Mechanics of Solder Materials

Abstract Chapter 2 reviews the fundamental theory on mechanics of solder materials. As solder materials are subject to high operating temperatures relative to their melting point, the thermo-mechanical deformation response of the solder is dependent on both temperature and strain-rate conditions. Hence, the theory on mechanics of solder materials will focus on elastic-plastic-creep and viscoplastic models for describing the thermo-mechanical deformation response of lead-free solder materials operating over a wide range of temperatures (-40°C to $+125^{\circ}\text{C}$) and strain rates ($0.0001\text{--}1,000\text{ s}^{-1}$).

Solder materials in electronic packaging assemblies are subjected to thermo-mechanical loads during accelerated reliability tests and in service operation. Accelerated Thermal Cycling (ATC) tests subject the solder joints to extreme temperatures; for example from -40°C to $+125^{\circ}\text{C}$. Such cyclic thermo-mechanical induced deformations in the package assembly cause the solder material to develop severe cyclic inelastic strains and cumulative fatigue damage resulting in failure of the solder joints [1, 2].

The stress, strain, and strain energy density components in solder materials can be computed numerically, if the governing material constitutive model has been developed from mechanics of materials tests. Materials testing and characterization of the elastic and inelastic deformation behavior are needed to derive the constitutive models to describe the solder deformation behavior in an elastic-plastic-creep model or a viscoplastic model approach [3].

Thermo-mechanical fatigue analysis in solder joints of electronic assemblies will require a stress and strain analysis approach and this often involves 2D and 3D modeling of the package assembly subject to the design or reliability test condition [4–6]. Fatigue damage driving force parameters such as stress-range, strain-range, and inelastic strain energy density per cycle can be computed and used in fatigue life prediction models.

2.1 Thermo-Mechanical Stress and Strain Analysis

An electronic package assembly is made up of different deformable materials joined by solder materials that undergo extensive amounts of deformations when subject to cyclic thermal loading. It is essential to understand the basic governing equations of thermo-mechanical strain in solder joints induced by mismatch in thermo-mechanical deformations [1, 2]. For a simple case, it can be assumed that the package is stress-free at a uniform temperature where there are no external or residual forces present. It is also assumed that the velocity and displacement of every element in the package at the instantaneous reference state is assumed to be small and the fundamental strain–displacement relation is given by,

$$\varepsilon_{ij} = \frac{1}{2} \left(\frac{\partial u_i}{\partial x_j} + \frac{\partial u_j}{\partial x_i} \right). \quad (2.1)$$

Hence, the governing equations for the isotropic thermal stresses for electronic packaging structure with steady-state heat flow condition ($\partial T / \partial t = 0$) are given by,

$$\delta_{ij} \frac{\partial}{\partial x_i} \left(\frac{\partial T}{\partial x_j} \right) = 0 \quad (2.2)$$

$$\sigma_{ij} = \lambda \varepsilon_{kk} \delta_{ij} + 2G \varepsilon_{ij} - \beta \delta_{ij} (T - T_0) \quad (2.3)$$

with the multi-axial strain components in a solid element given by,

$$\varepsilon_x = \frac{\partial u}{\partial x}, \quad \varepsilon_y = \frac{\partial v}{\partial y}, \quad \varepsilon_z = \frac{\partial w}{\partial z} \quad (2.4)$$

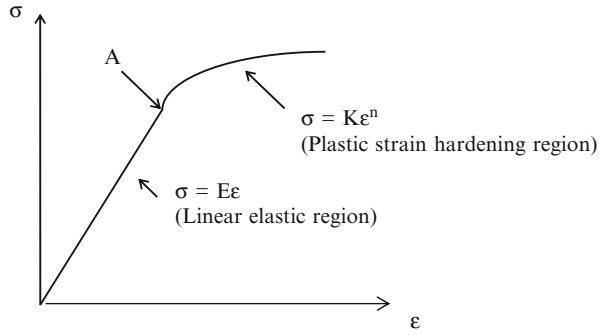
$$\gamma_{xy} = \frac{\partial u}{\partial y} + \frac{\partial v}{\partial x}, \quad \gamma_{yz} = \frac{\partial v}{\partial z} + \frac{\partial w}{\partial y}, \quad \gamma_{xz} = \frac{\partial w}{\partial x} + \frac{\partial u}{\partial z} \quad (2.5)$$

In three-dimensional analysis, a solid is subjected to multi-axial states of stresses and strains. The principal stresses and strains in the three principal planes, 1, 2, and 3 can be computed from a mechanics of materials analysis or by a numerical modeling approach employing a finite element analysis (FEA) method.

$$\sigma_1 > \sigma_2 > \sigma_3 \text{ and } \varepsilon_1 > \varepsilon_2 > \varepsilon_3,$$

where σ_1 , σ_2 , and σ_3 are the principal stresses, and ε_1 , ε_2 , and ε_3 are the principal strains at an element.

The equivalent *von Mises* stress equation is a yield criterion and is used to determine if the Yield stress state at the onset of plastic yielding has occurred in a solid element.

Fig. 2.1 Elastic-plastic stress–strain curve plot

$$\sigma^e = \frac{1}{\sqrt{2}} \left[(\sigma_1 - \sigma_2)^2 + (\sigma_2 - \sigma_3)^2 + (\sigma_3 - \sigma_1)^2 \right]^{1/2} \quad (2.6)$$

Similarly, the equivalent *von Mises* strain equation is used to compute the corresponding equivalent strain at the onset of plastic yielding and beyond.

$$\epsilon^e = \frac{\sqrt{2}}{3} \left[(\epsilon_1 - \epsilon_2)^2 + (\epsilon_2 - \epsilon_3)^2 + (\epsilon_3 - \epsilon_1)^2 \right]^{1/2} \quad (2.7)$$

In soldered electronic assemblies, the shear strain components are particularly important due to thermal expansion mismatch shear deformations in solder joints. The effective shear stress and shear strain can be derived from the equivalent *von Mises* stress and strain by:
effective shear stress,

$$\tau^* = \frac{1}{\sqrt{3}} \sigma^e \quad (2.8)$$

and effective shear strain,

$$\gamma^* = \sqrt{3} \epsilon^e. \quad (2.9)$$

The multi-axial stress and strain state at any point in a three-dimensional solid element can be resolved down to an equivalent stress and strain state using the *von Mises* stress–strain equation. This can then be related to the tensile test stress and strain response for modeling the elastic-plastic stress–strain curve behavior of a ductile material shown in Fig. 2.1.

The linear elastic region can be modeled by Hooke's law where stress (σ) and strain (ϵ) is related by Young's Modulus (E).

$$\sigma = E\epsilon \quad (2.10)$$

The plastic strain hardening region can be modeled by a time-independent non-linear stress–strain relationship,

$$\sigma = K\varepsilon^n \quad (2.11)$$

The plastic strain hardening region can be modeled as an isotropic or kinematic hardening material. Isotropic hardening assumes that the origin of the *von Mises* yield surface remains stationary in the stress space and the size of its yield surface expand resulting from strain hardening. In kinematic hardening, the *von Mises* yield surface does not change in size, but the origin of the yield surface is allowed to translate in the stress space to model strain hardening effects of increasing plastic flow stress. For solder materials, the tensile stress and strain curves are dependent on the test temperature and strain rate. The elastic modulus, yield strength, and ultimate tensile strength (UTS) properties vary with temperature and strain rate.

For a typical thermal cycling test from -40°C to 125°C , these mechanical properties reduce with the increase in temperature [7]. At -40°C to 125°C , a lead-free SAC solder material has a homologous temperature range of 0.5–0.8 of its melting point temperature of 217°C or 490 K. Creep deformation behavior in a solder material is highly dependent on the stress and temperature state. An elastic-plastic-creep constitutive model or viscoplastic constitutive model is needed to facilitate finite element modeling and simulation of solder joint reliability subject to thermal cycling tests [8].

2.2 Elastic-Plastic-Creep Model

Elastic-plastic-creep analysis [8] treats the total strain as the sum of the phenomenological components of elastic strain, time-independent plastic strain and time-dependent creep strain as shown below.

$$\varepsilon_{ij} = \varepsilon_{ij}^e + \varepsilon_{ij}^p + \varepsilon_{ij}^c \quad (2.12)$$

where ε_{ij} , ε_{ij}^e , ε_{ij}^p , and ε_{ij}^c are total, elastic, time-independent plastic and time-dependent creep strain tensors, respectively.

The total strain can be divided into an elastic component, ε_{el} , a time-independent plastic component, ε_{pl} , and a time-dependent creep component, ε_{cr} . The secant modulus can be expressed as:

$$\frac{1}{E_{sec}} = \frac{\varepsilon_{tot}}{\sigma} = \frac{\varepsilon_{el}}{\sigma} + \frac{\varepsilon_{pl}}{\sigma} + \frac{\varepsilon_{cr}}{\sigma} = \frac{1}{E_{el}} + \frac{1}{E_{pl}} + \frac{1}{E_{cr}} \quad (2.13)$$

From (2.13), it is noted that by increasing the strain rate, the contribution of the time dependent creep strain decreases such that for an infinite strain rate, ε_{cr} and $1/E_{cr}$ tend towards zero. Similarly, by decreasing the stress level of taking the slope on the stress-strain curve to calculate secant modulus, the contribution of the time-independent plastic strain decreases so that at a stress level small enough, any plastic effects can be eliminated, such that ε_{pl} and $1/E_{pl}$ tend towards zero. Therefore, only the elastic component is left and this results in giving the true Elastic modulus.

2.2.1 Temperature and Strain-Rate Dependent Elastic Modulus

The constitutive model [9, 10] for the apparent Elastic modulus can be written as

$$E(T, \dot{\varepsilon}) = (a_0 T + a_1) \log(\dot{\varepsilon}) + (a_2 T + a_3) + \delta, \quad (2.14)$$

where $\dot{\varepsilon}$ is the strain rate; T is the temperature; a_0 , a_1 , a_2 , and a_3 are constants; δ is the error term, which is introduced to account for any experimental error.

For constant temperature, two temperature-dependent constants $\alpha(T) = a_0 T + a_1$ and $\beta(T) = a_2 T + a_3$, can be introduced.

Equation (2.14) can then be written as

$$E = \alpha(T) \log(\dot{\varepsilon}) + \beta(T) + \delta \quad (2.15)$$

From (2.15), we can get the linear estimator equation:

$$\widehat{E} = \widehat{\alpha} \log(\dot{\varepsilon}) + \widehat{\beta}, \quad (2.16)$$

where \widehat{E} , $\widehat{\alpha}$, $\widehat{\beta}$ are estimated values of E , α , and β , respectively.

It is necessary to rewrite (2.16) in matrix notation in the form

$$Y = X \times C \quad (2.17)$$

and apply multiple linear regression with,

$$Y = \begin{bmatrix} E_1 \\ E_2 \\ \vdots \\ E_n \end{bmatrix} \quad X = \begin{bmatrix} \log(\dot{\varepsilon}_1) & 1 \\ \log(\dot{\varepsilon}_2) & 1 \\ \vdots & \vdots \\ \log(\dot{\varepsilon}_n) & 1 \end{bmatrix} \quad C = \begin{bmatrix} \alpha \\ \beta \end{bmatrix} \quad (2.18)$$

Using the experimental data, the temperature-dependent constants can be derived from calculus, where the estimated coefficient matrix, \widehat{C} , can be found from (2.19)

$$\widehat{C} = (X^T X)^{-1} X^T Y, \quad (2.19)$$

where $\hat{C} = \begin{bmatrix} \hat{a} \\ \hat{\beta} \end{bmatrix}$. Then the temperature-dependent constants α, β also can be expressed by the matrix notation forms

$$\begin{cases} Y_1 = X_1 \times C_1 \\ Y_2 = X_2 \times C_2 \end{cases}, \quad (2.20)$$

where

$$Y_1 = \begin{bmatrix} \alpha_1 \\ \alpha_2 \\ \alpha_3 \end{bmatrix} \quad X_1 = \begin{bmatrix} T_1 & 1 \\ T_2 & 1 \\ T_3 & 1 \end{bmatrix} \quad C_1 = \begin{bmatrix} a_0 \\ a_1 \end{bmatrix}$$

$$Y_2 = \begin{bmatrix} \beta_1 \\ \beta_2 \\ \beta_3 \end{bmatrix} \quad X_2 = \begin{bmatrix} T_1 & 1 \\ T_2 & 1 \\ T_3 & 1 \end{bmatrix} \quad C_2 = \begin{bmatrix} a_2 \\ a_3 \end{bmatrix}$$

Thus, the constants $a_0, a_1, a_2,$ and a_3 can be determined from calculus that estimated coefficient matrix, \hat{C}_1, \hat{C}_2 , are calculated as

$$\begin{aligned} \hat{C}_1 &= (X_1^T X_1)^{-1} X_1^T Y_1 \\ \hat{C}_2 &= (X_2^T X_2)^{-1} X_2^T Y_2, \end{aligned} \quad (2.21)$$

where

$$\hat{C}_1 = \begin{bmatrix} \hat{a}_0 \\ \hat{a}_1 \end{bmatrix}, \quad \hat{C}_2 = \begin{bmatrix} \hat{a}_2 \\ \hat{a}_3 \end{bmatrix} \quad (2.22)$$

By solving (2.19), (2.21), and (2.22) and substituting the solution of constants of $a_0, a_1, a_2,$ and a_3 into (2.14), the apparent Elastic modulus for 95.5Sn–3.8Ag–0.7Cu is obtained [7] as follows:

$$E(T, \dot{\epsilon})_{\text{SnAgCu}} = (-0.0005T + 6.4625) \log(\dot{\epsilon}) + (-0.2512T + 71.123) \quad (2.23)$$

2.2.2 Temperature and Strain-Rate Dependent Yield Stress and Ultimate Tensile Stress

The yield stress and UTS were established and expressed individually as follows:

$$\sigma_y(T, \dot{\epsilon}) = \alpha(T)(\dot{\epsilon})^{\beta(T)}, \quad (2.24)$$

where $\dot{\varepsilon}$ is the strain rate, T is the temperature, and

$$\begin{cases} \alpha(T) = b_0T + b_1 \\ \beta(T) = b_2T + b_3 \end{cases}$$

here b_0 , b_1 , b_2 , and b_3 are curve-fitted constants.

$$\text{UTS}(T, \dot{\varepsilon}) = \alpha(T)(\dot{\varepsilon})^{\beta(T)}, \quad (2.25)$$

where $\dot{\varepsilon}$ is the strain rate, T is the temperature, and

$$\begin{cases} \alpha(T) = c_0T + c_1 \\ \beta(T) = c_2T + c_3 \end{cases}$$

here c_0 , c_1 , c_2 , and c_3 are unknown constants.

Employing the same evolution procedure to determine the apparent Elastic modulus, the constants for yield stress and UTS can be determined [7] as follows:

$$\sigma_y(T, \dot{\varepsilon})_{\text{SnAgCu}} = (-0.2314T + 68.37)(\dot{\varepsilon})^{(2.29 \times 10^{-4}T + 0.0724)} \quad (2.26)$$

$$\text{UTS}(T, \dot{\varepsilon})_{\text{SnAgCu}} = (-0.2337T + 75.98)(\dot{\varepsilon})^{(2.5 \times 10^{-4}T + 0.0707)}. \quad (2.27)$$

The elastic modulus, yield stress, and UTS properties of solder materials are dependent on the temperature and strain rate of loading in a tensile test. Strain-rate hardening effects cause these properties to increase with the increase in strain rate from 10^{-5} s^{-1} to 10^{-1} s^{-1} [7, 11].

2.2.3 Ramberg-Osgood Model for Elastic-Plastic Stress–Strain Curve

One of the major goals of thermo-mechanical analysis in the electronics industry is to be able to model the stress–strain response in the solder joint and predict its reliability performance in design and in service.

A Ramberg-Osgood model describes the elastic-plastic behavior of solder materials very well and can be used to describe the stress–strain curve of solder tensile test results given by

$$\varepsilon = \frac{\sigma}{E} + \alpha \left(\frac{\sigma}{\sigma_0} \right)^n, \quad (2.28)$$

where n is the hardening exponent, α and σ_0 are material constants.

However for solder materials, the stress–strain curve is dependent on temperature and strain rate. Hence, a Modified Ramberg-Osgood model can be developed to include the temperature and strain-rate dependent effects.

2.2.4 Temperature and Strain-Rate Dependent Modified Ramberg-Osgood Model

The Ramberg-Osgood model hardening exponent n and stress coefficient σ_0 are modified to be temperature and strain-rate dependent for solder materials. The temperature and strain-rate dependent Modified Ramberg-Osgood model can be described as

$$\varepsilon(T, \dot{\varepsilon}) = \frac{\sigma}{E} + \alpha \left(\frac{\sigma}{\sigma_0(T, \dot{\varepsilon})} \right)^{n(T, \dot{\varepsilon})}. \quad (2.29)$$

From the tensile test result, the mechanical properties have a linear relationship with temperature and logarithmic relationship with strain rate. So formation of temperature and strain-rate dependent n and σ_0 can be written as

$$\sigma_0(T, \dot{\varepsilon}) = \sigma_0 + aT^* + b\dot{\varepsilon}^* \quad (2.30)$$

$$n(T, \dot{\varepsilon}) = n + cT^* + d\dot{\varepsilon}^* \quad (2.31)$$

where $T^* = \frac{T - T_r}{T_m - T_r}$, $\dot{\varepsilon}^* = \ln\left(\frac{\dot{\varepsilon}}{\dot{\varepsilon}_r}\right)$, a and c are temperature coefficients, b and d are strain-rate coefficients. T_r and $\dot{\varepsilon}_r$ are reference temperature and strain rate, respectively. T_m is the melting temperature of Sn–3.8Ag–0.7Cu (217°C), n and σ_0 are hardening exponent and stress coefficient at the reference temperature and strain rate.

2.3 Creep Constitutive Models

Creep of a solder material is often characterized by its steady-state creep strain rate, $\dot{\varepsilon}_{ss}$, which can be simply expressed as power law relationship,

$$\dot{\varepsilon} = A\sigma^n e^{\frac{-Q}{KT}}, \quad (2.32)$$

where A is material constant, σ is applied stress, n is stress exponent, Q is creep activation energy, K is Boltzmann's constant, and T is absolute temperature. The activation energy, Q , and the stress exponent, n , change with the dominant creep mechanism and may have different values for different regimes of the applied stress.

By taking the natural logarithm, (2.32) can be rewritten as,

$$\ln \dot{\epsilon} = \ln A + n \ln \sigma - \frac{Q}{K} \frac{1}{T} \quad (2.33)$$

It can be seen from (2.33) that for the creep process under the controlling constant stress, the creep deformation mechanism does not change at small temperature range. Therefore, the activation energy, Q , could be determined from the slope of the, $\ln \dot{\epsilon}$ versus $1/T$ plot.

To describe the steady-state creep strain rate over a wider regime of stresses and temperatures, a hyperbolic-sine creep model is often used for solder materials [11]. The steady-state creep strain rate for intermediate to high stress power law breakdown regime is:

$$\dot{\epsilon} = C[\sinh(\alpha\sigma)]^n \exp\left(-\frac{Q}{KT}\right), \quad (2.34)$$

where $\dot{\epsilon}_c$ = equivalent creep strain rate (s^{-1}), σ = equivalent *von Mises* stress (N/mm^2), T = absolute temperature (kelvin), C is a constant, α is the stress level at which the power law dependence breaks down, n is the stress exponent for dislocation glide-controlled kinetics, Q is the activation energy for creep deformation process, and K is the Boltzmann's constant.

The elastic-plastic-creep approach is a phenomenological way to describe the constitutive behavior of solder alloy, since the elastic, plastic and creep strains represent different deformation. For thermo-mechanical cyclic loading, the time-independent plastic strain and time-dependent creep strain can be readily computed from an elastic-plastic-creep analysis using FEA modeling and simulation [12, 13]. Another useful method from a state variable approach of inelastic strain is the viscoplastic strain analysis approach. This method combines the creep and plastic strain components as a unified state variable inelastic strain.

2.4 Viscoplastic Constitutive Model

The viscoplastic model approach follows the materials perspective that dislocation motion is the cause of both creep and plastic deformation [8, 13], and combined them into inelastic strain. A viscoplastic model that has been used for modeling rate-dependent deformation behavior of ductile metals is the Anand viscoplastic model, which was originally reported by Anand [14] and Brown et al. [15]. The Anand viscoplastic model was applied to tin-lead solder joints subject to thermal cycling loading by Darveaux [16]. The Anand viscoplastic model was curve fitted for lead-free tin-silver (Sn-3.5Ag) and tin-silver-copper (SAC387) solder alloys, respectively [12, 17].

The total strain is expressed as,

$$\varepsilon_{ij} = \varepsilon_{ij}^e + \varepsilon_{ij}^{\text{in}}, \quad (2.35)$$

where $\varepsilon_{ij}^{\text{in}}$ is the inelastic strain tensor.

The Anand model consists of two coupled differential equations that relate the inelastic strain rate to the rate of deformation resistance.

The strain rate equation is represented by,

$$\frac{d\varepsilon_{\text{in}}}{dt} = A \left[\sin h \left(\xi \frac{\sigma}{s} \right) \right]^{\frac{1}{m}} \exp (-Q/RT) \quad (2.36)$$

The rate of deformation resistance is given by

$$\dot{s} = \left\{ h_0 (|B|)^{\alpha} \frac{B}{|B|} \right\} \frac{d\varepsilon_p}{dt} \quad (2.37)$$

$$B = 1 - \frac{s}{s^*} \quad (2.38)$$

$$s^* = \hat{s} \left[\frac{1}{A} \frac{d\varepsilon_p}{dt} \exp (-Q/RT) \right], \quad (2.39)$$

where $d\varepsilon_{\text{in}}/dt$ is the effective inelastic strain rate, σ is effective true stress, s is the deformation resistance, T is the absolute temperature, A is pre-exponential factor, ξ is stress multiplier, m is strain rate sensitivity of stress, Q is activation energy, R is universal gas constant, h_0 is hardening/softening constant, \hat{s} is coefficient for deformation resistance saturation value, n is strain-rate sensitivity of saturation value, and α is strain-rate sensitivity of hardening or softening.

In the Anand model, (2.36) deals with the relationship between saturation stress and strain rate under certain temperatures. Equations (2.37)–(2.39) deal with the hardening and softening flow response where the relationship between strain and stress can be computed over a range of strain rate and temperature.

The saturation stress in (2.40) can be derived from (2.36) as follows:

$$\sigma^* = \frac{\hat{s}}{\xi} \left(\frac{\dot{\varepsilon}_p}{A} e^{Q/RT} \right)^n \sin h^{-1} \left[\left(\frac{\dot{\varepsilon}_p}{A} e^{Q/RT} \right)^m \right], \quad (2.40)$$

where $\dot{\varepsilon}_p$ and T denote strain rate and temperature, respectively.

The parameters Q/R , A , \hat{s}/ξ , m , and n can be determined by a nonlinear fitting method to steady-state creep strain rate test data.

The relationship between the viscoplastic stress and inelastic strain is given by,

$$\sigma = \sigma^* - [(\sigma^* - c s_0)^{(1-a)} + (a-1) c h_0 \sigma^{*(-a)} \varepsilon_p]^{1/(1-a)}. \quad (2.41)$$

Table 2.1 Anand model parameters for 63Sn–37Pb solder

A	Q/R	ξ	m	n	\hat{s}	s_0	h_0
26	5,797	10	0.256	0.043	83.1	38	921.48

The variable ε_p is the nonlinear strain, and a , s_0 and h_0 are parameters to be determined, where c is a function of strain rate and temperature given in (2.42).

$$c \equiv \frac{1}{\xi} \sin h^{-1} \left[\left(\frac{\dot{\varepsilon}_p}{A} e^{Q/RT} \right)^m \right] \quad c < 1. \quad (2.42)$$

The values of the nine material parameters Q , A , \hat{s} , ξ , m , n , a , s_0 , and h_0 for any given solder alloy can be determined by the curve-fitting procedures given below:

1. Determination of the saturation stress σ^* under a series of strain rate and temperature by creep test.
2. Curve fitting of parameters Q/R , A , \hat{s}/ξ , m , and n in (2.40).
3. Determination of ξ and \hat{s} . For value of \hat{s}/ξ has been determined in step (2), value of ξ should be estimated such that the value of c will match condition: $c < 1$. And then the value of \hat{s} can be derived from \hat{s}/ξ and the estimate of ξ .
4. Curve fitting of a , s_0 , and h_0 in (2.41).

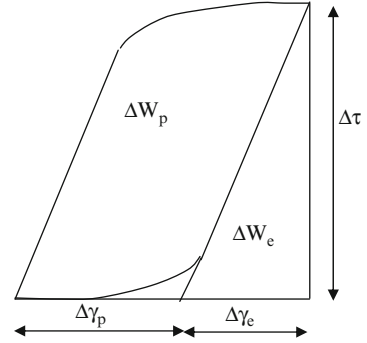
For example, the above curve-fitting method for the Anand viscoplastic model was applied to tensile and creep test data for 63Sn–37Pb solder alloy. Tensile test data for three different temperatures, 25°C, 75°C, and 125°C, and three states of strain rate, 5.6E–2, 5.6E–3, and 5.6E–4, were used. Table 2.1 shows the result of the nine parameters of the Anand viscoplastic model for 63Sn–67Pb solder.

2.5 Fatigue Life Prediction Models for Solder Materials

Thermo-mechanical fatigue failure in solder joints subject to thermal cycling tend to fail in the Low Cycle Fatigue (LCF) range where the fatigue life to failure falls between 100 and 10,000 thermal cycles. The fatigue life prediction models to be used depends on the fatigue test condition and fatigue damage parameters used. The fatigue damage driving force parameters such as the plastic strain-range, creep strain range and inelastic strain energy density per cycle can be used in different fatigue life prediction models.

The LCF approach can be based on the strain or energy parameter used to characterize the fatigue failure process [18–20]. These parameters are (a) plastic strain range, (b) creep strain range and (c) inelastic energy. The strain range-based fatigue approach employs low cycle strain-controlled fatigue test method. The inelastic strain comprises of the plastic strain range and creep strain range. The plastic shear strain deformation is represented by the time-independent plastic

Fig. 2.2 Cyclic stress–strain hysteresis loop



strain component, while the creep strain component contributes to the time-dependent inelastic strain included in the plastic shear strain ($\Delta\gamma_p$) component as shown in Fig. 2.2. The energy-based fatigue model employs the cyclic stress–strain hysteresis loop to compute the elastic strain energy density (ΔW_e) and inelastic dissipated energy or plastic work per cycle (ΔW_p).

2.5.1 Plastic Strain Range Fatigue Models

The Coffin–Manson fatigue model [18] is perhaps the best-known and most widely used approach for LCF analysis. The total number of cycles to failure, N_f , is dependent on the plastic strain range, $\Delta\epsilon_p$, the fatigue ductility coefficient, ϵ'_f , and the fatigue ductility exponent, c , given in the expression below:

$$\frac{\Delta\epsilon_p}{2} = \epsilon'_f (2N_f)^c. \quad (2.43)$$

The fatigue ductility coefficient, ϵ'_f , is approximately equal to the true fracture ductility, ϵ_f . The fatigue ductility exponent, c , varies between -0.5 and -0.7 [21], and experimental data are required to determine the constants.

Solomon's LCF model [22] relates the plastic shear strain range to fatigue life cycles is given below:

$$\Delta\gamma_p N_p^\alpha = \theta \quad (2.44)$$

$\Delta\gamma_p$ is the plastic shear strain range. N_p is the number of cycles to failure, θ is the inverse of the fatigue ductility coefficient, and α is a material constant.

2.5.2 Creep Strain Range Fatigue Models

Creep strain range fatigue models account strictly for the cyclic creep deformation in the solder joints. Early attempts at modeling creep were made by isolating the elastic and plastic deformation mechanisms. Creep, as mentioned previously, can be separated into two possible mechanisms, matrix and grain boundary creep. Knecht and Fox [23] proposed a simple matrix creep fatigue model relating the solder microstructure and the matrix creep shear strain range given below,

$$N_f = \frac{C}{\Delta\gamma_{mc}} \quad (2.45)$$

The number of cycles to failure, N_f , is related to a constant C , which is dependent on failure criteria and solder microstructure. $\Delta\gamma_{mc}$ is the strain range due to matrix creep.

2.5.3 Creep-Fatigue Interaction Model

By applying Miner's linear superposition principal, both plastic and creep strain can be accounted for in strain-based fatigue model [24]. This model combines the Solomon fatigue model with the Knecht and Fox creep model and is given below:

$$\frac{1}{N_f} = \frac{1}{N_p} + \frac{1}{N_c}, \quad (2.46)$$

where N_p refers to the number of cycles to failure due to plastic fatigue and is obtained directly from the Solomon's fatigue model, N_c refers to the number of cycles to failure due to the creep fatigue and is obtained from the Knecht and Fox's creep fatigue model.

2.5.4 Frequency Modified Plastic Strain Range Method

The constants in the Coffin–Manson model are dependent on temperature and cyclic frequency. The modified Coffin–Manson model [25] given below:

$$\left[N_f v^{(k-1)} \right]^m \Delta\epsilon_p = C, \quad (2.47)$$

where

$$v^{(k-1)} = \begin{cases} v^{(k_1-1)} & \text{for } 1 \text{ Hz} \geq v \geq 10^{-3} \text{ Hz} \\ \left[\frac{v}{10^{-3}} \right]^{(k_2-1)} (10^{-3})^{(k_1-1)} & \text{for } 10^{-3} \text{ Hz} > v \geq 10^{-4} \text{ Hz} \end{cases}$$

and, k_1 , k_2 , m , and C are dependent on temperature and frequency. The frequency effect was compensated by this frequency-modified model. However, the temperature effect of LCF behavior is still a problem.

2.5.5 Energy-Based Models

Energy-based fatigue models form the largest group of models. These models are used to predict fatigue failure based on a hysteresis energy term or type of volume-weighted average stress-strain history.

A modified energy-based LCF model [26], is given below,

$$\left[N_f v^{(k-1)} \right]^m \frac{W_p}{2\sigma_f} = C, \quad (2.48)$$

where

$$v^{(k-1)} = \begin{cases} v^{(k_1-1)} & \text{for } 1 \text{ Hz} \geq v \geq 10^{-3} \text{ Hz} \\ \left[\frac{v}{10^{-3}} \right]^{(k_2-1)} (10^{-3})^{(k_1-1)} & \text{for } 10^{-3} \text{ Hz} > v \geq 10^{-4} \text{ Hz} \end{cases}$$

and, k_1 , k_2 , m , and C are dependent on temperature and frequency.

An empirical plastic work model was developed by Darveaux [2, 16] for solder joint subject to thermal cycling tests and is used to predict the crack initiation and crack growth behavior using the equations given below:

$$N_0 = K_1 \Delta W^{K_2} \quad (2.49)$$

$$\frac{da}{dN} = K_3 \Delta W^{K_4}, \quad (2.50)$$

where ΔW is the plastic work, a is the area of the solder joint where a fatigue crack will grow till failure, K_1 , K_2 , K_3 , and K_4 are constants fitted to the test data. This model must be used with a calibrated FEA model with a specific element size and volume.

The plastic work, ΔW , calculated must be normalized by the volume of the solder elements used for fatigue analysis.

$$\Delta W_{\text{ave}} = \frac{\sum \Delta W \cdot V}{\sum V}, \quad (2.51)$$

where ΔW_{ave} is the average plastic work and V is the volume of each element selected for analysis.

References

1. Lau JH (1993) Thermal stress strain in microelectronics packaging. New York: Van Nostrand Reinhold
2. Lau JH (1991) Solder joint reliability, theory and application. New York, Van Nostrand Reinhold
3. Pang HLJ (2007) Lead-free solder materials: design for reliability, Chapter 12. In: Suhir E, Lee YC, Wong CP (eds) Micro- and opto-electronic materials and structures: physics, mechanics, design, reliability, packaging, vol 7, Materials physics/materials mechanics. Springer, New York
4. Pang JHL, Chong DYR (2001) Flip chip on board solder joint reliability analysis using 2-D and 3-D FEA models. IEEE Trans Adv Packag 24(4):499–506
5. Pang JHL, Chong DYR, Low TH (2001) Thermal cycling analysis of flip-chip solder joint reliability. IEEE Trans Components Packag Technol 24(4):705–712
6. Pang JHL, Low TH, Xiong BS, Che FX (2003) Design for reliability (DFR) methodology for electronic Packaging assemblies. Proceedings of IEEE, 2003 Electronics Packaging Technology Conference, pp 470–478
7. Pang JHL, Xiong BS (2005) Mechanical properties for 95.5Sn-3.8Ag-0.7Cu lead-free solder alloy. IEEE Trans Components Packag Technol 28(4):830–840
8. Yeo A, Lee C, Pang HLJ (2006) Flip chip solder joint reliability analysis using viscoplastic and elastic-plastic-creep analysis. IEEE Trans Components Packag Technol 29(2):355–363
9. Shi XQ, Pang HLJ, Zhou W, Wang ZP (1999) Temperature and strain rate effects on mechanical properties of 63Sn/37Pb solder alloy. Advances in Electronic Packaging 1999, Proceedings of InterPACK'99, pp 551–557
10. Shi XQ, Zhou W, Pang HLJ et al (1999) Effect of temperature and strain rate on mechanical properties of 63Sn/37Pb solder alloy. ASME J Electron Packag 121(3):179–185
11. Pang JHL, Xiong BS, Low TH (2004) Creep and fatigue characterization of lead free 95.5Sn-3.8Ag-0.7Cu solder. Proceedings of IEEE, 2004 Electronic Components and Technology Conference, 54th ECTC, vol 2, pp 1333–1337
12. Pang JHL, Yeo A, Low TH, Che FX (2004) Lead-free 96.5Sn-3.5Ag flip chip solder joint reliability analysis. Proceedings of IEEE, 2004 Inter Society Conference on Thermal Phenomena, ITherm 2004, vol 2, pp 160–164
13. Che FX, Pang JHL (2004) Thermal fatigue reliability analysis for PBGA with Sn-3.8Ag-0.7Cu solder joints. 2004 Proceedings of Electronics Packaging Technology Conference, pp 787–792
14. Anand L (1985) Constitutive equations for hot working of metals. J Plasticity 1:213–231
15. Brown SB, Kwon HK, Anand L (1989) An internal variable constitutive model for hot working of metals. Int J Plastic 5:95–130
16. Darveaux R (2000) Effect of simulation methodology on solder joint crack growth correlation. Electronic Components and Technology Conference, 2000 IEEE, pp 158–169

17. Che FX, Pang JHL, Xiong BS, Xu L, Low TH (2005) Lead free solder joint reliability characterization for PBGA, PQFP and TSSOP assemblies. 2005 Proceedings of 55th Electronic Components and Technology Conference, pp 916–921
18. Coffin LF (1954) A study of the effects of cyclic thermal stresses on a ductile metal. *Trans ASME* 76:931
19. Manson SS (1965) Fatigue a complex subject-some simple approximations. *Exp Mech* 5 (7):193–226
20. Morrow JD (1964) Cyclic plastic strain energy and fatigue of metals. ASTM STP 378, American Society for Testing and Materials, Philadelphia, PA, p 45
21. Kilinski TJ, Lesniak JR, Sandor BI (1991) Modern approaches to fatigue life prediction of SMT solder joints. In: Lau JH (ed) *Solder joint reliability theory and applications*. Van Nostrand Reinhold, New York
22. Solomon HD (1991) Predicting thermal and mechanical fatigue lives from isothermal low cycle data, Chapter 14. In: Lau JH (ed) *Solder joint reliability*. Van Nostrand Reinhold, New York
23. Knecht S, Fox R (1990) Constitutive relationship and creep-fatigue life model for eutectic tin-lead solder. *IEEE Trans Components, Hybrids, and Manufacturing Technol* 13(2):424–433
24. Pang JHL, Seetoh CW, Wang ZP (2000) CBGA solder joint reliability evaluation based on elastic-plastic-creep analysis. *J Electron Packag* 122:255–261
25. Shi XQ, Pang HLJ, Zhou W, Wang ZP (2000) Low cycle fatigue analysis of temperature and frequency effects in eutectic solder alloy. *Int J Fatigue* 22:217–228
26. Shi XQ, Pang HLJ, Zhou W, Wang ZP (1999) A modified energy-based low cycle fatigue model for eutectic solder alloy. *Scr Mater* 41(3):289–296

Lead Free Solder

Mechanics and Reliability

Pang, J.H.L.

2012, X, 175 p. 162 illus., Hardcover

ISBN: 978-1-4614-0462-0